Article

Optically Modulated and Optically Activated Delayed Fluorescent Proteins through Dark State Engineering

Published as part of The Journal of Physical Chemistry virtual special issue "W. E. Moerner Festschrift".

Baijie Peng, Ryan Dikdan, Shannon E. Hill, Athéna C. Patterson-Orazem, Raquel L. Lieberman, Christoph J. Fahrni, and Robert M. Dickson*

Read Online

ACCESS | Metrics & More | Article Recommendations | Supporting Information

ABSTRACT: Modulating fluorescent protein emission holds great potential for increasing readout sensitivity for applications in biological imaging and detection. Here, we identify and engineer optically modulated yellow fluorescent proteins (EYFP, originally 10C, but renamed EYFP later, and mVenus) to yield new emitters with distinct modulation profiles and unique, optically gated, delayed fluorescence. The parent YFPs are individually modulatable through secondary illumination, depopulating a long-lived dark state to dynamically increase fluorescence. A single point mutation introduced near the chromophore in each of these YFPs provides access to a second, even longer-lived modulatable dark state, while a different double mutant renders EYFP unmodulatable. The naturally occurring dark state in the parent YFPs yields strong fluorescence modulation upon long-wavelength-induced dark state depopulation, allowing selective detection at the frequency at which the long wavelength secondary laser is intensity modulated. Distinct from photoswitches, however, this near IR secondary coexcitation repumps the emissive S_1 level from the long-lived triplet state, resulting in optically activated delayed fluorescence (OADF). This OADF results from secondary laser-induced, reverse intersystem crossing (RISC), producing additional nanosecond-lived, visible fluorescence that is delayed by many microseconds after the primary excitation has turned off. Mutation of the parent chromophore environment opens an additional modulation pathway that avoids the OADF-producing triplet state, resulting in a second, much longer-lived, modulatable dark state. These Optically Modulated and Optically Activated Delayed Fluorescent Proteins (OMFPs and OADFPs) are thus excellent for background- and reference-free, high sensitivity cellular imaging, but time-gated OADF offers a second modality for true background-free detection. Our combined structural and spectroscopic data not only gives additional mechanistic details for designing optically modulated fluorescent proteins but also provides the opportunity to distinguish similarly emitting OMFPs through OADF and through their unique modulation spectra.
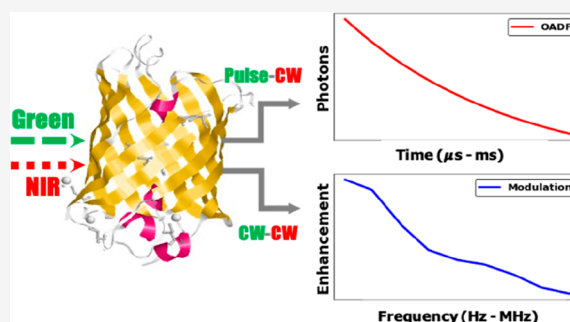
INTRODUCTION

Yellow fluorescent proteins (YFPs) are pivotal to biological research, as they yield bright emission in a relatively low-background spectral window. YFPs, as a spectral class, are among the brightest and most versatile genetically encoded fluorophores,[3] which makes them essential in multilabel/multicolor imaging schemes.[4] As EYFP (10C,[1] but renamed EYFP later[2]) results from only four point mutations (S65G, V68L, S72A, and T203Y) of green fluorescent protein (GFP),[5−8] tuning the immediate chromophore environment tailors spectral and photophysical properties for a wide array of imaging applications.[9−11] While both electronic[5] and steric[12,13] interactions are known to alter emission, longer wavelength emission typically comes from an anionic chromophore, often facilitated through ground or excited state proton transfer pathways,[14] while photoswitching tends to result from cis−trans isomerization.[12,13,15] Although genetically optimized for

bright emission, fluorescent proteins (FPs) also exhibit multiple dark states that enable new imaging modalities.[16−22] The multiple states in EYFP, for example, were demonstrated to be optically interconvertible, even on the single molecule level,[8] laying the groundwork for many advances in super-resolution fluorescence and high-sensitivity imaging. Thus, both proton transfer and isomerization are crucial to FP photophysics and guide design of dark and bright states within FPs,[23] while giving rise to many of their novel applications.[15,24]

Recently, background suppression through optically modulating residence of photopopulated dark states has led to selectivity and sensitivity gains in fluorescence imaging and detection.[25−27] Such gains result from dynamically altering ground state population with intensity-modulated, very long-wavelength coillumination to depopulate dark states faster than they naturally decay. This optically induced dark state depopulation then increases primary-induced fluorescence as the ground state population increases. Turning the secondary laser on and off at a specific frequency encodes this modulation waveform on the collected fluorescence, allowing its selective detection at a specific lock-in frequency, with essentially no background noise. Such dual-laser modulation and signal recovery schemes have yielded up to 100-fold sensitivity improvements[27] and have been demonstrated in emission from organic dyes,[28,29] few-atom Ag clusters,[27,30] and optically modulated fluorescent proteins (OMFPs),[31] while also improving photoacoustic imaging sensitivity.[32] In each of these cases, whether in animal or cellular imaging, no additional background signal was generated since the secondary wavelength was much lower energy than the fluorescence collection window,[25,26] and signals are readily separated. While the secondary laser intensity most directly controls the dark state population, modulation depth also depends on the dark state lifetime. Thus, modulating at too high a frequency prevents bright and dark state steady-state populations from being established. This means that each fluorophore can be distinguished based on its modulation frequency response, and the dark state lifetime can be used as an extra resolving dimension in fluorescence imaging, even when emitters have identical emission spectra.[18,31]

We have identified several OMFPs that, upon photo-excitation, transiently reside in μs- to ms-lived dark states that can be depopulated by lower energy coillumination.[25] To date, only blue fluorescent proteins (BFPs)[33] and Aequorea coerulescens GFP (AcGFP)[31] have been shown to be optically modulatable. Photoswitchable FPs (PS-FPs) can also give background-free detection by modulating both primary and secondary lasers and detecting at the sum and difference of the modulation frequencies,[34] or by using sequential excitation conditions.[19] In each case, demodulating OMFP fluorescence results in background suppression and drastic signal enhancements over autofluorescence and, in some cases, resolution of bound vs unbound OMFPs through kinetic resolution.[34] The palette of OMFPs would benefit from expansion to other colors and modification of the chromophore surroundings to further tune dark state lifetimes. While this background-suppressed demodulated fluorescence is highly advantageous for biological imaging, especially in high background,[26] the mechanism by which OMFPs produce modulated emission, and the range of emitters distinguishable solely on dark state lifetimes, remains to be explored.[31] Herein, we generate new, modulatable YFPs to better understand the photophysical and structural bases of their modulatable emission.

EXPERIMENTAL METHODS

Directed Evolution of EFYP. Site-directed saturation mutagenesis of EYFP residues Gly65, His148, and Ser205 was performed by a combination of overlap extension PCR and error-prone PCR (epPCR). Normal PCRs were performed with EconoTaq PLUS 2X master mix (Lucigen), and epPCRs were performed with Taq polymerase, which lacks endo and exonuclease activities. Sequences for the corresponding flanking primers and internal primers are provided in the Supporting Information. The internal mutagenic primers contained a randomized codon for all amino acid possibilities at the respective residue sites. PCR was performed on each fragment of EYFP to incorporate the randomized codons. The EYFP fragments were then sequentially combined via overlap extension PCR followed by PCR amplification with outer primers. Error prone PCR was performed in the presence of manganese chloride and an uneven ratio of nucleotides.[35] The products were digested, ligated into a pBAD expression vector, and transformed into TOP10 chemically competent E. coli (Invitrogen). Cells were plated on 0.002% arabinose LB +ampicillin so that the EYFP variants would be uniquely expressed in each colony. After transformation, plates were incubated overnight and subsequently stored either at room temperature for 1 day or at 4 °C, until fluorescence was detectable in the individual colonies.

Screening of EYFP Mutants. Colonies that were visibly fluorescent upon white light illumination were picked into individual wells of a 96 deep-well plate containing 1 mL of 0.002% arabinose LB+ampicillin each. The plate was covered with parafilm and incubated at 30 °C with shaking at 250 rpm overnight. A 50-μL sample of each culture was combined with 50 μL of 50% glycerol to make a glycerol stock plate, which was stored at −80 °C. The deep-well plate cultures were spun down, the media was removed, and the pellets were lysed by addition of 100 μL of Bacterial Protein Expression Reagent (B-PER, ThermoFisher Scientific). The plate was vortexed and then centrifuged to separate the insoluble from the soluble lysate. The soluble lysate was then diluted 1:100 into PBS. The diluted soluble lysate was screened in glass-bottom 96-well plates on an inverted optical microscope for modulation using 514.5 nm continuous wave (CW) primary and 705 nm secondary excitations focused into each well. The positive control for alignment and modulation was the parent OMFP strain, EYFP. A total of 288 wells, each, in principle containing a unique mutant (but due to random mutagenesis, some may have been duplicates) were screened for fluorescence and modulation differences from the parent EYFP. For a given alignment and primary and secondary excitation intensities, modulation frequency was scanned to measure the characteristic frequency response that correlates to dark state life-times.[18,25,29] Secondary laser modulation frequency was scanned from 1 Hz to 100 kHz, and modulation depth was monitored through measuring the amplitude at the modulation frequency upon Fourier transformation of fluorescence intensity vs time. Modulatable mutants with differing dark state lifetimes, increased modulation depth, additional modulatable dark states, or no observable modulation were identified. Identified proteins of interest were then overexpressed and either purified by affinity chromatography using a 6xHis tag (see below) or studied in cell lysate. Absorption spectra of overexpressed proteins were acquired using a UV-2401 PC spectrophotometer (Shimadzu), and fluorescence spectra were acquired on a Photon Technology International QuantaMaster spectrofluorimeter.

Protein Expression and Purification. To generate expression vectors for identified point mutants, a pBAD vector with an EYFP or mVenus insert and N-terminal 6xHis tag was mutated using the Q5 Site Directed Mutagenesis kit (New England BioLabs). The mutants generated were the EYFP/ H148S, EYFP/K52R, EYFP/H148S/K52R, EYFP/G65 V/ S205T, EYFP/G65 V/H148S, EYFP/H148S/S205T, and

mVenus/H148S, all of which were verified by sequencing. The plasmids were transformed into chemically competent *E. coli* TOP10 cells. Single colonies were used to inoculate 100 mL of LB ampicillin + 0.002% arabinose and grown overnight at 37 °C with shaking at 250 rpm. The cultures were pelleted and lysed using B-PER (ThermoFisher Scientific). The resulting lysate was run through a 1 mL HisTrap FF Nickel affinity column (GE Healthcare) on an ÄKTAprime chromatography system. Purity was confirmed by SDS-PAGE, and the protein fractions were combined, concentrated, and buffer exchanged into PBS by using a concentration device with a 10 kDa molecular weight cut off (MWCO) filter.

Fluorescence Characterization and Modulation Measurements. Microscopy was performed on an inverted microscope (Olympus IX70 or IX71) with a 40× air objective (Olympus, 0.65 NA). All solution data were recorded by focusing the excitation laser ∼30 μm into the PBS-buffered, pH 7.4 protein solution. Purified protein emission and modulation depth and frequency response were confirmed to be similar at pH 7 and pH 8 to ensure that modulation differences were not a result of any pH-induced changes to the chromophore. Fluorescence signal was collected using a confocal microscope arrangement with a 100-μm multimode fiber (Thorlabs) serving as the pinhole and directing the signal to a photon-counting avalanche photodiode (APD, Perkin-Elmer or Excelitas). Collected photon intensity trajectories were recorded using a PCI-6602 Counter (National Instruments). A line-tunable argon ion laser (514.5 nm, Coherent) or a diode laser (517.5 nm, Thorlabs) was used as the continuous wave (CW) primary excitation. Several diode lasers (Thorlabs) were available as secondary excitations. Primary and secondary laser beams were combined using a dichroic mirror so that they were spatially overlapped while entering the microscope and focused onto the sample. Appropriate band-pass filters centered near the emission wavelengths of EYFP were used to block both primary and secondary laser wavelengths. Sinusoidal modulation of the secondary laser intensity was performed by modulating the laser diode (Thorlabs, LDC series) driving current with a function generator (Agilent or Berkeley Nucleonics). Excitation intensities under dual laser excitation for EYFP/H148S and EYFP were optimized for highest enhancement (Figure S1). Proteins showed optimal enhancement for primary laser intensities between 0.5 and 1 kW/cm^2 and secondary laser intensities of ∼10 kW/cm^2. Dual laser modulation experiments on all YFPs were performed with these intensities, unless otherwise specified. The EYFP/H148S fluorescence quantum yield was measured against fluorescein at pH 7.4 as a reference, and its extinction coefficient at 513 nm was measured on separate occasions, both through comparison to the 1.0 M NaOH-denatured chromophore absorption (447 nm, 44 000 M^{-1}cm^{-1})[36] to determine protein concentration and from absorption measurements of known concentration solutions.

OADF Measurement. OADF measurements were performed on purified YFPs in PBS solutions. Either a pulsed laser (532 nm, ∼100 ps pulse width, PicoQuant) or a CW laser (517.5 nm, Thorlabs) with pulse width modulation (acousto-optic modulator, NEOs) was used for primary excitation, and an 830 nm CW diode laser (Thorlabs), for secondary excitation. Collected photon intensity trajectories were recorded using a PCI-6602 Counter (National Instruments). The time-tagged photons after each primary laser pulse were binned and overlaid into a microtime histogram for delayed

fluorescence detection and analysis. Time traces were collected with and without secondary coillumination, and secondary laser intensity was varied to determine dark state lifetimes for OADF. Emission filters block both primary and secondary excitation sources while collecting emission only within the normal fluorescence spectral window.

Data Analysis. Fluorescence time traces were binned at a rate at least 2.5 times higher than the secondary laser modulation rate. A fast Fourier transform (FFT) was performed on the time trace, and its amplitude at the modulation frequency in the Fourier domain (FFT magnitude) was recorded. The FFT magnitude was divided by the amplitude at zero frequency and doubled to determine the enhancement (accounting for equal amplitude peaks at positive and negative modulation frequencies yielded by FFT).

X-ray Crystallography. Prior to crystallization, EYFP/H148S was exchanged into 50 mM Hepes pH 7.5 by twice concentrating and diluting in a 15 mL 10K MWCO Amicon Ultracentrifugation device, to a final concentration of 18.7 mg/mL. A 3-μL hanging drop (1:1 ratio protein/mother liquor) was equilibrated against 1 mL of mother liquor composed of 1.75 M Na/K phosphate pH 6.9 at room temperature in a Styrofoam box, optimized from published conditions.[5] Although no crystals were observed after 3 months, a yellow plate-like cluster was apparent after ∼10 months. This crystal was harvested and cryocooled in a mother liquor solution supplemented with 15% glycerol. Diffraction data were collected at the Southeast Regional Collaborative Access Team (SER-CAT) beamline 22-ID at the Advanced Photon Source (Argonne National Laboratory). Data were processed in space group *P*1 using HKL2000,[37] resulting in a 3.6 Å resolution data set. The structure was solved by molecular replacement in Phenix[38] using a monomer from the protein data bank (PDB) code 3 V3D as the search model. Eight molecules were identified in the asymmetric unit. Although relatively low resolution, the histidine mutation was apparent in the electron density map (Supplemental Figure S2). During refinement, reference restraints with 3V3D and noncrystallographic symmetry across the polypeptide chains of each monomer were used. Crystallographic statistics are presented in Table S1. Superpositions with wild-type (WT) YFP (PDB code 1YFP) and asFP595 (PDB code 2A54) were accomplished in Coot[39] using secondary structure matching.[40] Figures were generated in the open-source version of PyMOL (www.pymol.org).[41] The structure was deposited to the PDB with accession code 6VIO.

■ RESULTS AND DISCUSSION

EYFP Dark States. EYFP was shown to have at least two dark states that lead to both stochastic blinking and high-energy photoswitching/photorecovery.[8] Exciting EFYP fluorescence at 514.5 nm, we investigated depopulating the thermally unstable state giving rise to ms-lived blinking by coilluminating EYFP at 705 nm. EYFP fluorescence arises from primary laser excitation at rate k_{exc}, with some small fraction (Φ_{dark}) populating the dark state from S$_1$. Rather than waiting for the dark state lifetime $\tau_{\text{dark}} = k_{\text{off}}^{-1}$, long-wavelength secondary laser illumination more rapidly depopulates the dark state to regenerate the fluorescent manifold and increase the primary-excited fluorescence. Modulating the secondary laser encodes the modulation waveform on the collected fluorescence, enabling the background-suppressed signal of interest to be selectively recovered from Fourier transformed

fluorescence time traces and ultimately be used in image reconstruction.

Yellow fluorescence increased significantly with both lasers illuminating the sample, but secondary illumination alone generates no fluorescence, as it is a longer wavelength than that of collected yellow emission. Modulating the secondary laser intensity in the dual laser scheme, however, modulates yellow fluorescence with an enhancement (fluorescence increase upon dual laser illumination, normalized by primary laser-only excited fluorescence) of up to 60% (Figure 1, green curve).
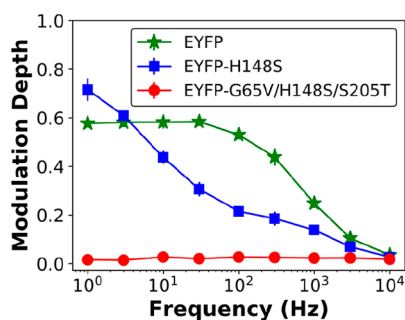
Figure 1. Frequency response curves for EYFP and its mutants. According to the modulation profiles, EYFP/H148S (blue) shows an additional longer-lived dark state, while G65 V/H148S/S205T (red) is not modulatable.

Operationally, this is calculated as twice the Fourier amplitude at the modulation frequency (to account for the equal amplitude peaks at positive and negative frequency), divided by the zero-frequency amplitude for a pure (zero background) emitter. EYFP enhancement is significantly higher than that of AcGFP, which showed only ~12% fluorescence enhancement.[31] The magnitude of enhancement (or the modulation depth) is the fraction of fluorescence signal that can be shifted from zero modulation frequency (where all unmodulatable background appears) to a unique, essentially background-free detection window. Higher modulation depths thereby produce increased sensitivity in high background imaging. Because background emitters have not been observed to be modulatable, even using low modulation frequency shifts OMFP signals away from all background emitters to selectively recover OMFP-labeled features.

Modulation depth decreases at high modulation frequencies as steady-state populations cannot be fully established during on and off periods that are shorter than the finite dark state lifetime. For a single dark state, OMFP modulation depth, m, vs modulation frequency (ν, Hz) is described by $m = A/\sqrt{1 + (2\pi\nu\tau)^2}$, where A is a constant and τ is the characteristic lifetime. The characteristic frequency, $\nu_c = \tau^{-1}$, is the sum of the intensity-dependent rate constants out of and back into the emissive manifold of states, $k_{on} + k_{off}$, and corresponds to a modulation depth falling to $(1 + 4\pi^2)^{-1/2}$ of its original value (i.e., $\nu_c\tau = 1$) as modulation frequency, ν, is increased. Characteristic EYFP modulation frequency curves (Figure 1) suggest ν_c is ~1.7 kHz, indicating a single dark state lifetime on the order of ~1 ms. The similarity in blinking time scale suggests that the modulatable state is the same as that identified in the original single-molecule studies[8] that gives rise to fluorescence intermittency or blinking. The previously observed photoswitching process[8] appears unaffected by long

wavelength coillumination, as it required 405 nm excitation to regenerate the fluorescent state.

Generation and Initial Characterization of New YFP Variants. Using our prior BFP studies[33] as a guide, we mutated residues at positions 65, 148, and 205 in EYFP and assessed any changes in modulation characteristics. The residues His148 and Ser205 around the EYFP fluorophore are crucial to forming the proton wire linking the chromophore hydroxy group to the surrounding amino acids.[42] From this approach, two distinct EYFP mutants, H148S and G65 V/S205T, were identified as exhibiting unique modulation profiles. The modulation profile for the parent EYFP indicates that it has only a single ~ms-lived dark state lifetime component, whereas the EYFP/H148S mutant displays an additional long-lifetime component. In contrast, the double mutant EYFP/G65V/S205T is fluorescent, but not modulatable (Figure S3). While the single mutation H148S is responsible for introducing a second, long-lived modulatable dark state into EYFP, both the G65V and S205T mutations are needed to remove modulation, as each of the two double mutants EYFP/G65V/H148S and EYFP/H148S/S205T is modulatable with modulation spectra that are quite similar to that of the single mutant EYFP/H148S (Figure S3).

As all modulatable EYFP mutants show a very similar ~kHz characteristic modulation frequency, we initially studied this faster-decaying dark state in EYFP. Mutation near the chromophore preserves this fast modulation time scale while introducing an additional, more slowly decaying modulatable dark state. The commonality of this shorter-lived modulatable dark state suggests that it may be more electronic in origin, as mutations near the chromophore do not significantly alter its time scale.

Characterization of the Shorter-Lived YFP Dark State. The natural off time, or lifetime of the dark state, can be obtained by measuring the characteristic frequency as a function of primary CW intensity. As the characteristic frequency is the sum of the rates into and out of the dark state, extrapolating the characteristic intensity to zero primary intensity yields the natural off time as the y-intercept. Plotting the characteristic frequency as the secondary laser is modulated vs primary CW intensity for EFYP yields a characteristic off rate of ~1.7 kHz, or a dark state lifetime of ~0.59 ms (Figure 2). This time scale could result from a wide range of photophysical processes. The most common for organic dyes would be formation of a triplet state, but these typically occur with a low yield and exhibit a shorter μs-lifetime. In contrast to organic dyes, however, the FP chromophore is well-protected from dioxygen within the FP β-barrel,[43] making population of a triplet state[44,45] a possibility for this ~ms-lived dark state.

We recently showed that one contribution to overall enhancement in organic dyes and Ag nanocluster emitters can result from efficient triplet state population.[29,46,47] In this case, secondary laser-induced reverse intersystem crossing can repopulate the emissive S_1 state to generate additional fluorescence long after the primary pulse has passed. Such Optically Activated Delayed Fluorescence (OADF) is most readily observed using pulsed primary and CW secondary illumination. After the primary pulse has passed, ns-lived, visible emission results from secondary, near-IR excitation of the primary laser-prepared triplet state. Such secondary-excited emission decays over many microseconds and requires no further primary excitation. Resulting from triplet shelving and low energy, optically induced recovery of the S_1 state, OADF is
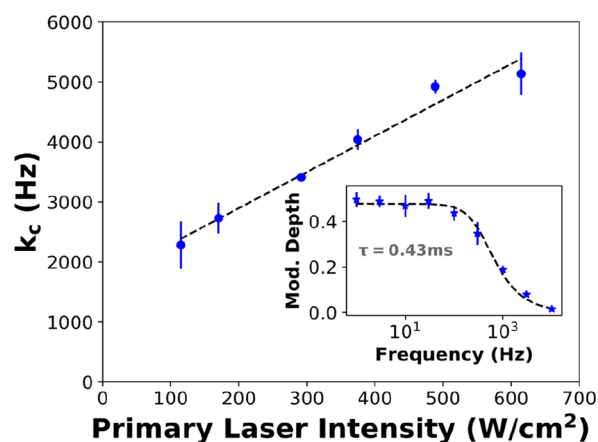
Figure 2. Characteristic frequencies (k_c) of EYFP are plotted as a function of CW 515 nm primary and 808 nm secondary excitation intensities. The y-intercept yields the natural dark state decay rate (k_{off}^0) of the fluorophore, which is 1700 ± 190 Hz. Inset: EYFP modulation depth as a function of modulation frequency fit to the phase-resolved lifetime equation $m = A/\sqrt{1 + (2\pi\nu\tau)^2}$. Modulation was performed with a 515 nm primary laser (~150 W/cm^2) and 808 nm secondary laser, which results in a τ of 0.43 ± 0.04 ms.

a clear indication of the triplet level being the modulatable dark state, while also providing a new path for generating background-free emission and elucidating photophysical constants.[29,46,47] Interestingly, while OADF indicates triplet state involvement, the majority of enhancement results not from the OADF photons, but from faster repopulation of the S_0 state for increased fluorescence excitation cycles within the fluorescent manifold.

To probe this shorter-lived (~0.59 ms) dark state in both EYFP and EYFP/H148S, we illuminated each sample with pulsed primary (532 nm, 100 ps pulse width) and CW secondary (830 nm) illumination. Prompt, ~2 ns-lived fluorescence results from primary excitation, but when near-IR, CW secondary illumination is present, very slowly decaying yellow fluorescence is observed between the primary pulses (Figure 3). This clear signature of OADF results from a long-lived dark state being populated that naturally decays on the μs to ms time scale, but coillumination in the near IR regenerates

the emissive S_1 level through reverse intersystem crossing, causing it to decay faster than its natural lifetime. Increased secondary intensity increases the OADF decay, which is fit to a single exponential decay profile. Plotting OADF decay constant vs secondary intensity yields a straight line, with the intercept again giving the natural dark state decay (or the inverse of the triplet lifetime, Figure 3c). For both EYFP and EYFP/H148S, which share a strikingly similar time scale in their modulation frequency spectra, this extrapolates to a similar ~0.5 ms triplet lifetime (Figure 3c). Note that the shorter dark state lifetime observed under CW primary excitation (Figure 2) results from nonzero dark state absorption of the primary laser. CW-CW enhancement decreases with increased CW primary intensity as the primary excitation begins to directly depopulate the dark state, decreasing measured enhancement attributable to secondary laser illumination (Figure S1). Pulsed primary excitation removes the primary-induced depopulation channel, as only the secondary laser illuminates the dark state between primary pulses. While somewhat long-lived for a triplet state, the fluorescent protein β-barrel is known to shield the FP chromophore from dioxygen, which would increase the triplet lifetime. Further, Franck−Condon overlaps must be strong to enable radiative relaxation after low-energy secondary illumination, indicating the dark state (1) must not be photoisomerized and (2) must be electronically excited.

OADF from YFP Triplet States. Using very narrow primary pulses (~100 ps) approximates impulse excitation (pulse width is short relative to the fluorescence lifetime). Thus, such short primary excitation is sufficiently narrow relative to the ~2 ns fluorescence lifetime to largely prevent each FP from being excited more than once per primary pulse. CW secondary illumination accelerates the depopulation of the triplet state, as natural triplet decay is quite slow. Thus, the integrated OADF (I-OADF) is a good approximation of the triplet population and, for impulse primary excitation, the ratio of I-OADF to prompt fluorescence should approximate, but not exceed, the triplet quantum yield.[29,46] The I-OADF to prompt fluorescence ratios for EYFP and EYFP/H148S thereby indicate Φ_T's of ~0.3%. OADF generates additional photons through repumping the emissive S_1 level through RISC, but, after OADF emission, the ground state ends up
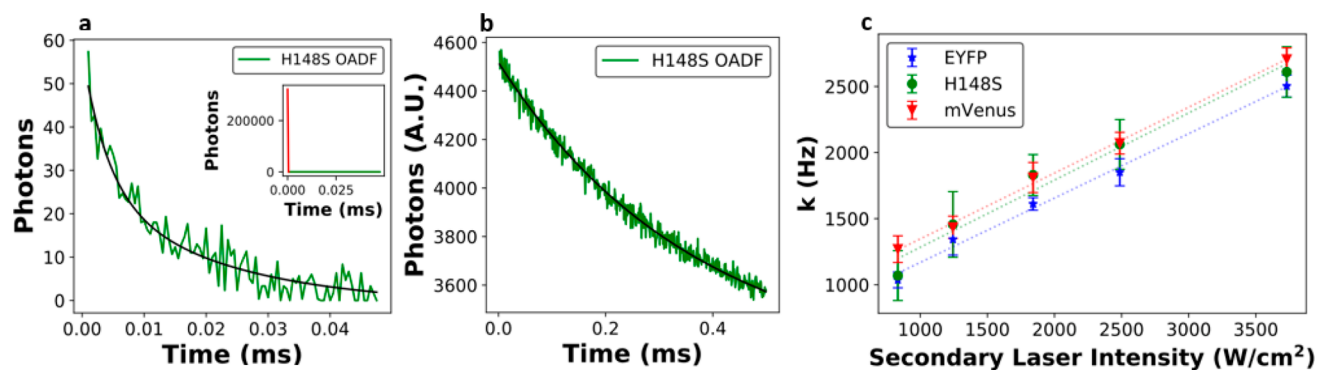
Figure 3. (a) Binned time-trace plot for pulsed primary and continuous secondary OADF measurement on EYFP/H148S, the integrated area from secondary illumination after the primary pulse has passed (photons from the primary pulse are shown in the inset as the red portion of the curve). High secondary intensity (~10 kW/cm^2 at 800 nm) was used to maximize OADF intensity, but gives a fast OADF decay (~10 μs). The OADF/prompt fluorescence ratio is ~0.0035. (b) Binned OADF time trace data from the H148S mutant at lower secondary intensity (~3.7 kW/cm^2 at 800 nm), yielding a longer OADF lifetime of ~0.37 ms after initial 532 nm-excited prompt fluorescence. (c) EYFP, the H148S mutant, and mVenus (another YFP variant) all show OADF decays that are linear with secondary laser intensity at 830 nm.
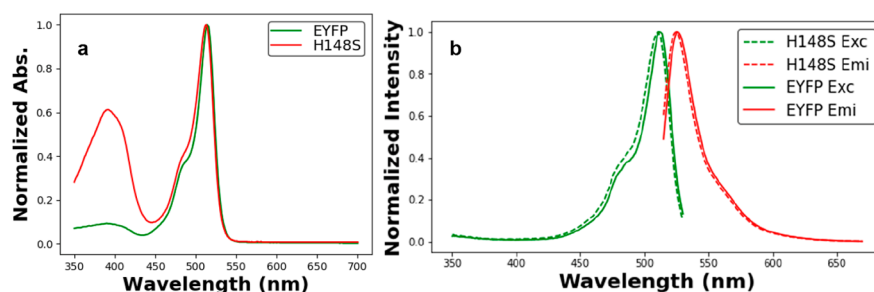
Figure 4. (a) Normalized absorbance spectra for EYFP and H148S mutant. A blue absorption band (~395 nm) in the H148S mutant relative to its parent EYFP is observed. The two absorptions in H148S yield a lower extinction coefficient at 513 nm (~28 000 M^{-1}cm^{-1}) relative to that of EYFP/10C parent (36,500 M^{-1}cm^{-1}).[1,2] (b) Excitation (530 nm emission) and emission spectra (513 nm excitation) for H148S and parent EYFP/10C.

being repopulated faster than through natural triplet decay. Thus, both OADF and additional primary-excited fluorescence contribute to the enhancement, with the latter dominating the overall enhancement.

To increase triplet population and corresponding OADF, we excited each YFP with burst CW primary excitation and CW secondary illumination. Burst-CW primary excitation enables multiple excitations of each YFP during each primary pulse, yielding higher steady-state triplet populations and increased relative OADF. As there is a competing dark state in the H148S mutant, EYFP exhibits much greater relative gains in the I-OADF/prompt fluorescence ratio under these excitation conditions. Utilizing an externally modulated diode laser for primary excitation, we adjusted the 515 nm burst width from 200 ns to 25 μs and recorded OADF upon CW 705 nm coillumination. In this burst-CW excitation, the I-OADF:integrated prompt fluorescence ratio (0.0011) is comparable to that for pulsed-CW excitation (Figure 3, 0.0035), but the I-OADF:average prompt fluorescence/bin ratio (0.30) is much larger due to dark state buildup during the longer primary burst pulse. Although H148S has an additional dark state, burst primary excitation significantly increases steady-state triplet state population and the relative OADF contribution, which appears on zero background. The OADF decay after each primary pulse was fit to an exponential decay, $I(t) = Ae^{(-t/\tau)}$,[47] where t is the time after the pulse, τ is the OADF lifetime, and A is a pre-exponential factor. The OADF decay rate is dependent on secondary intensity, and the y-intercept when plotting τ^{-1} vs secondary intensity gives the natural triplet decay rate (Figure 3c).

Additional Longer-Lived Dark State in H148S Mutant. Although OADF clearly involves triplet shelving and RISC, the majority of modulation processes reported to date result from faster restoration of the ground state population for continued primary excitation. Such ground state recovery occurs with OADF, but it also occurs upon photoinduced interconversion between ground state photoisomers. As isomerization can be coupled with tautomerization, such a state could be consistent with enhancement from a longer-lived dark state that does not exhibit OADF, as Franck–Condon overlaps between cis and trans ground states are expected to be poor. Such photoisomerization and ground state tautomerization is a mechanism by which much longer-lived dark states enable photoswitching in FPs, and is a good candidate for the longer-lived states introduced upon mutation, as long as the photoisomer experiences steric hindrance to reversion that kinetically traps it. Electronic changes around

the isomerized chromophore could then facilitate longer-wavelength absorption.

Fitting the EYFP/H148S modulation spectrum to a two-component decay, the two obtained time scales are 0.40 ± 0.18 ms and 24 ± 2 ms (Figure S4). As noted above, the faster time scale is very similar to that of the parent EYFP, but the second is much slower and is consistent with a photoisomer. As this longer-lived dark state shows no OADF, but does yield strong modulation when excited at long wavelength, we suggest that this is a ground state photoisomer, but that the electronic interactions with the environment are changed to enable long-wavelength (secondary) absorption. Thus, both electronics and sterics would be expected to be changed by the H148S mutation, altering the stabilities and interconversion of the cis and trans chromophoric forms.

As H148 is close to the YFP chromophore, we expected it to have a similar effect on both EYFP and on the similarly modulatable YFP, mVenus. Thus, modulation of both mVenus and mVenus/H148S were characterized. Like EYFP, mVenus shows a single ~0.5 ms-lived, strongly modulatable dark state that yields significant OADF with a dark state decay constant that is linear with secondary laser intensity (Figure 3c). Like EYFP, mVenus/H148, also exhibits this same fast modulation time scale as well as an additional longer-lived, ~100 ms modulatable dark state (Figure S5). Thus, all modulatable YFPs exhibit OADF with similar time scales, presumably from their triplet levels and long-wavelength induced reverse intersystem crossing. Introduction of the H148S mutation in either mutant, however, adds an additional, long-lived, modulatable dark state that likely results from steric effects on the FP chromophore.

Ground State Absorption Spectra. Comparing the ground state absorption spectra of EYFP and EYFP/H148S reveals a more pronounced blue absorption band in the H148S mutant relative to its parent EYFP (Figure 4). In the reversibly switchable protein rsGreen, this same H148S mutation was shown to be involved in an extended hydrogen bond network involved in switching between neutral trans and anionic cis chromophore states.[48] Although chromophore isomerization can alter the time scales of modulation or introduce new processes, the cis vs trans forms of the chromophore should give little to no spectral shift.[13] It is the neutral and anionic forms of the chromophore that produce the blue and green absorption, respectively.[14,49] The larger blue absorption in EYFP/H148S than in the parent EYFP lends further support to the idea that the EYFP/H148S mutant exists in both anionic and neutral forms. The new modulatable state introduced with an ~24 ms lifetime, however, also suggests that isomerization
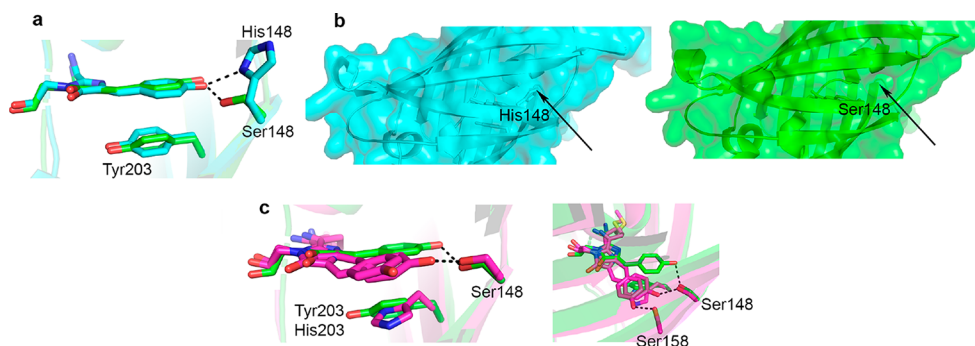
Figure 5. Crystal structure of EYFP/His148Ser (green) in comparison with WT EYFP (cyan) and asFP595 (magenta). (a) Zoomed in view of chromophore in EYFP/H148S and WT EYFP. Both His148 and Ser148 are within H-bonding distance of the chromophore hydroxy group. (b) Molecular surface in the vicinity of His148/Ser148 is distinct in the two structures, with a deep pocket in EYFP/H148S that is occluded in WT EYFP (arrow). (c) Comparison of EYFP/H148S with asFP595, in which the chromophore appears in two trans conformations. In asFP595, one conformation (left) forms a H-bonding interaction with Ser148, whereas, in the other (right), an interaction with Ser158 is observed. In EYFP/H148S, Phe165 (not shown) is at the position of Ser158 in asFP595. Dashed black lines: atoms within hydrogen-bonding distance (2.6−3.5 Å).

in the EYFP/H148S mutant contributes to the properties of this new state. Thus, the neutral trans form is seen as being more likely to form in EYFP/H148S, and the 24-ms-lived dark state introduced with the H148S mutation, coupled with the structural differences, lead to the conclusion that the anionic cis form of the EYFP/H148S chromophore is less well-stabilized than in the parent, leading to a more pronounced role of the photoinduced cis−trans isomerization and the formation of the neutral trans chromophore as the additional EYFP/H148S dark state. Because of the significant lifetime differences within the H148S mutant, the two dark states are clearly distinguished in the frequency domain (Figure 1).

Structure of EYFP/H148S. To gain insight into structural modifications that might account for the slower modulation time scale upon introduction of Ser148, we solved the 3.6 Å crystal structure of EYFP/H148S. Even though the data set is of medium-resolution, it is a starting point for comparison to published structures. First, replacing His148 in the parent EYFP structure (PDB code 1YFP) with Ser does not change the H-bonding distance with the hydroxy group of the chromophore (both ∼2.8 Å, Figure 5a). With less steric bulk with Ser present in EYFP/H148S compared to His in the parent EYFP, a new molecular surface is apparent (Figure 5b). This extra space likely allows for photoisomerization of the chromophore. The trans conformation of the chromophore is expected to be populated at a relatively low level given steric clash with Phe165 and other nearby hydrophobic residues, unlike asFP595 (PDB code 2A54),[50] where the photo-isomerized trans form of the chromophore is stabilized by Ser158, the residue at the equivalent position of Phe165 in EYFP/H148S (Figure 5c). Thus, the structure supports the proposal that the longer-lived modulatable state involves photoisomerization of the EYFP/H148S chromophore, while the OADF-generating, shorter-lived modulatable state is similar to that in the parent EYFP and results from modulating the triplet state.

Simulation of YFP Fluorescence. As modulation can result both from OADF and from increasing prompt fluorescence through optically induced ground state recovery, we simulated YFP fluorescence through a 4-state model using the rate matrix in eq 1 corresponding to the Jablonski diagram in Figure 6. The experimental I-OADF/prompt fluorescence ratios were used as estimates of the triplet quantum yields. Photophysical parameters were adjusted to match published
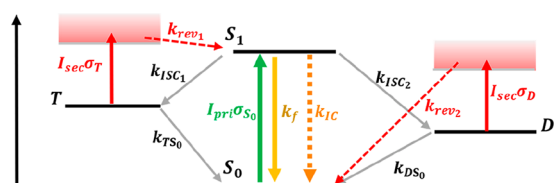
Figure 6. Photophysics for the modulatable YFPs. EYFP and mVenus have only one shorter-lived state (labeled T), which is likely a triplet state and can be optically converted to S_1, resulting in delayed fluorescence. The H148S mutants exhibit the additional longer-lived dark state, D, which is likely a photoisomer state. For H148S, the green primary excitation yields bright yellow fluorescence and can populate the T and D states. Near IR secondary excitation repopulates the S_0 ground state from both T and D, but only some of the re-excitation of T goes through S_1 to produce yellow OADF.

and experimental values while also reproducing our optical modulation and OADF experimental results. As experimental rates vary in time with changing illumination conditions (i.e., time-varying primary and secondary intensities), the rate matrix was piecewise exponentiated. While at least 10× time resolution for each laser pulse width was used, logarithmic time steps were employed to speed up calculations and reduce memory usage. S_1 state population at each time step was used as a surrogate for fluorescence intensity. Integration of fluorescence from each process (often having different bin resolutions) was performed as a midpoint Riemann sum for each of the differently sized bins. Simulations with and without secondary illumination enable calculation of the relative contributions of OADF and increased prompt fluorescence to the overall enhancement.

$$\frac{d}{dt}\begin{pmatrix} S_0 \\ S_1 \\ T \\ D \end{pmatrix} = \begin{pmatrix} -I_{pri}\sigma_{S_0}\frac{\lambda}{hc} & k_f & k_{TS_0} & k_{DS_0}^0 + k_{DS_0} \\ I_{pri}\sigma_{S_0}\frac{\lambda}{hc} & -k_{S_1D} - k_{S_1T} - k_f & k_{TS_1} & 0 \\ 0 & k_{S_1T} & -k_{TS_0} - k_{TS_1} & 0 \\ 0 & k_{S_1D} & 0 & -k_{DS_0}^0 - k_{DS_0} \end{pmatrix} \begin{pmatrix} S_0 \\ S_1 \\ T \\ D \end{pmatrix} \quad (1)$$

In Figure 6 and eq 1, the pairs of subscripts in the rate constants (k) and reverse quantum yield (Φ_{rev}) indicate the conversion between dark (T or D) and bright (S_0 or S_1) states. The initial states are on the left, and the final states are on the right. The isomer dark state D is depopulated at a natural decay rate $k_{DS_0}^0$. When the secondary laser is on, the dark state, D, is depopulated with an additional rate k_{DS_0}, which can also be described by $I_{sec}[t]\sigma_D\Phi_{revDS_0}\lambda h^{-1}c^{-1}$. Analogous expressions

Table 1. Photophysical Parameters Used for H148S Simulation[a]

Parameter	Φ_F	$\Phi_T (10^{-3})$	Φ_D	$\Phi_{revTS_0}\,\sigma_T$	$\Phi_{revDS_0}\,\sigma_D$	$\tau_{offD_1}^0$	$\tau_{offD_2}^0$	σ_{S_0}
Value	0.59 ± 0.05	3.5 ± 0.6	8.0×10^{-5}	1.1×10^{-19}	2.45×10^{-20}	$0.025s$	$0.9s$	2.3×10^{-16}

[a]All absorption cross sections (σ) have units of cm^2/molecule. Φ_F of 0.63[2] was used in EYFP simulations.

are obtained for the triplet to singlet conversion by replacing the subscript D with T for triplet state parameters. The secondary laser has a wavelength λ and intensity $I_{sec}[t]$, σ_D is the dark state absorption cross section, Φ_{revDS_0} is the reverse quantum yield from the isomerized dark sate isomer to the ground state, and $\lambda h^{-1}c^{-1}$ converts the units to Hz. Similarly, the secondary laser depopulates the triplet state at a rate k_{TS_1}, which can be described by $I_{sec}\sigma_T\Phi_{revTS_1}\lambda h^{-1}c^{-1}$. Optimized simulation parameters that reproduce experimental modulation and OADF results (Figure 7) are given in Table 1.
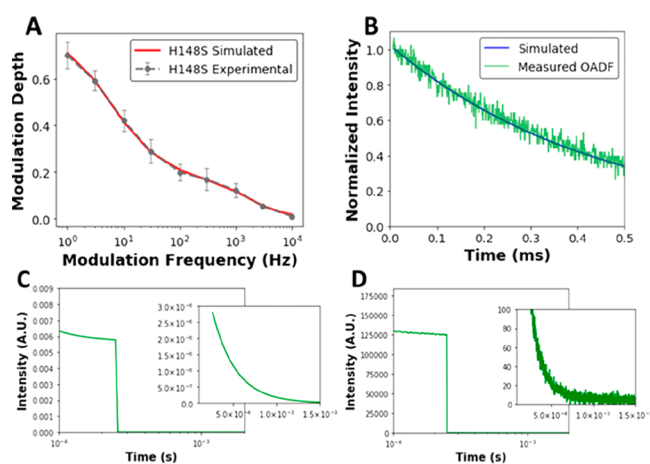
Figure 7. (A) Experimental and simulated modulated frequency response curves for EYFP/H148S. Both simulation and experiment were performed with 515 nm, 500 W/cm^2 primary and 800 nm, 12 kW/cm^2 secondary laser intensities. (B) Green: Measured binned time-trace plot for burst primary and continuous secondary (∼800 nm and ∼2500 W/cm^2) OADF for EYFP/H148S. Blue line: Simulated delayed fluorescence matching the experimental conditions using parameters specified in Table 1. (C) Simulated Burst-CW emission for EYFP-H148S with zoomed in region for showing OADF (inset). (D) Experimental Burst-CW traces collected with secondary intensity of ∼6 kW/cm^2. Inset shows experimental OADF. Simulated parameters in C correspond to those in Table 1 and experimental intensities in D.

While OADF is a small fraction of the total emission, the long-wavelength-induced repopulation of the ground state yields large (∼60%) enhancements relative to primary excitation alone. Thus, even though OADF appears small, it has a large effect on fluorescence enhancement and enables efficient background suppression through demodulating collected fluorescence. EYFP (and mVenus) parent proteins can be directly distinguished from their similarly emitting single H148S mutants by examining modulation depth vs modulation frequency as a new dark state is introduced, presumably involving photoisomerization. Structural and photophysical simulations support our experimental results and guide interpretations of this first observation of OADF and of optical modulation in YFPs.

CONCLUSION

Although dark state quantum yields are <1%, quantum yields into two competing dark states are directly measurable through modulated dual-laser excitation and fluorescence detection. Photophysical simulation of excitation and decay rates coupled to experimental conditions give state populations and signal strengths under varied excitation conditions, enabling significant dark state buildup. Through burst-CW primary excitation, fluorescent proteins are shown to have an optically modulatable triplet state that produces OADF through secondary laser-induced RISC. This excitation scheme not only produces completely background-free emission in a time window devoid of emission from other species but also regenerates the ground state to give additional modulation of primary-excited fluorescence. The overall modulation depths of the parent proteins EYFP and mVenus are seen to be on the order of 60% due to the combination of secondary laser-induced OADF and ground state repopulation, providing multiple modes of background-suppressed imaging (fluorescence demodulation or time-gated OADF detection). Utilizing site-directed saturation mutagenesis, we introduced an additional longer-lived dark state that appears to be coupled with isomerization and possible ground state tautomerization. The crystal structure of EYFP/H148S shows an opening up of the chromophore environment that may facilitate photoisomerization, without obvious stabilization of the trans isomer. As excitation deposits additional energy into the chromophore, the increased pocket size is likely to facilitate the cis−trans interconversion that leads to the additional optical modulation pathway. As this state is longer-lived than the triplet, it builds up population for longer times, decreasing, but not eliminating, modulation from the triplet state. The ∼1 kHz modulation component and OADF of EYFP and mVenus H148S mutants are both similar in time scale to those of the parents, but amplitudes are reduced as the isomer population is preferentially built up. Importantly, strongly emissive, but unmodulatable YFP mutants were also produced with different point mutations near the chromophore. These coupled optical, simulation, and structural studies all directly indicate the importance of the immediate chromophore environment and structure in altering fluorescent protein dark states and optical modulation of emission. The structural and electronic changes from mutagenesis can expand the dimensionality of FP imaging, offering a new path to tune modulation frequency response and depth for simultaneously detecting similarly emissive FPs based on the dark state lifetime.

ASSOCIATED CONTENT

Ⓢ Supporting Information

The Supporting Information is available free of charge at https://pubs.acs.org/doi/10.1021/acs.jpcb.1c00649.

Information containing fluorescent protein preparation and screening methods, and additional fluorescent protein modulation behaviors is provided. (PDF)

■ AUTHOR INFORMATION

Corresponding Author

    Robert M. Dickson − *School of Chemistry & Biochemistry and Petit Institute for Biosciences and Bioengineering, Georgia Institute of Technology, Atlanta, Georgia 30332-0400, United States;* ⊙ orcid.org/0000-0003-0042-6194; Email: dickson@chemistry.gatech.edu

Authors

    Baijie Peng − *School of Chemistry & Biochemistry and Petit Institute for Biosciences and Bioengineering, Georgia Institute of Technology, Atlanta, Georgia 30332-0400, United States*

    Ryan Dikdan − *School of Chemistry & Biochemistry and Petit Institute for Biosciences and Bioengineering, Georgia Institute of Technology, Atlanta, Georgia 30332-0400, United States*

    Shannon E. Hill − *School of Chemistry & Biochemistry and Petit Institute for Biosciences and Bioengineering, Georgia Institute of Technology, Atlanta, Georgia 30332-0400, United States*

    Athéna C. Patterson-Orazem − *School of Chemistry & Biochemistry and Petit Institute for Biosciences and Bioengineering, Georgia Institute of Technology, Atlanta, Georgia 30332-0400, United States*

    Raquel L. Lieberman − *School of Chemistry & Biochemistry and Petit Institute for Biosciences and Bioengineering, Georgia Institute of Technology, Atlanta, Georgia 30332-0400, United States;* ⊙ orcid.org/0000-0001-9345-3735

    Christoph J. Fahrni − *School of Chemistry & Biochemistry and Petit Institute for Biosciences and Bioengineering, Georgia Institute of Technology, Atlanta, Georgia 30332-0400, United States;* ⊙ orcid.org/0000-0003-3731-7434

Complete contact information is available at:
https://pubs.acs.org/10.1021/acs.jpcb.1c00649

Notes

The authors declare no competing financial interest.

■ REFERENCES

(1) Orm, M.; Cubitt, A. B.; Kallio, K.; Gross, L. A.; Tsien, R. Y.; Remington, S. J. Crystal Structure of the Aequorea Victoria Green Fluorescent Protein. *Science* **1996**, *273*, 1392−1395.

(2) Lybarger, L.; Dempsey, D.; Patterson, G. H.; Piston, D. W.; Kain, S. R.; Chervenak, R. Dual-Color Flow Cytometric Detection of Fluorescent Proteins Using Single-Laser (488-nm) Excitation. *Cytometry* **1998**, *31*, 147−152.

(3) Shaner, N. C.; Steinbach, P. A.; Tsien, R. Y. A Guide to Choosing Fluorescent Proteins. *Nat. Methods* **2005**, *2*, 905−909.

(4) Shaner, N. C.; Patterson, G. H.; Davidson, M. W. Advances in Fluorescent Protein Technology. *J. Cell Sci.* **2007**, *120*, 4247−4260.

(5) Wachter, R. M.; Elsliger, M.-A.; Kallio, K.; Hanson, G. T.; Remington, S. J. Structural Basis of Spectral Shifts in the Yellow-Emission Variants of Green Fluorescent Protein. *Structure* **1998**, *6*, 1267−1277.

(6) Giepmans, B. N. G.; Adams, S. R.; Ellisman, M. H.; Tsien, R. Y. Review - the Fluorescent Toolbox for Assessing Protein Location and Function. *Science* **2006**, *312*, 217−224.

(7) Perez-Jimenez, R.; Garcia-Manyes, S.; Ainavarapu, S. R. K.; Fernandez, J. M. Mechanical Unfolding Pathways of the Enhanced Yellow Fluorescent Protein Revealed by Single Molecule Force Spectroscopy. *J. Biol. Chem.* **2006**, *281*, 40010−40014.

(8) Dickson, R. M.; Cubitt, A. B.; Tsien, R. Y.; Moerner, W. E. On/Off Blinking and Switching Behaviour of Single Molecules of Green Fluorescent Protein. *Nature* **1997**, *388*, 355.

(9) Chalfie, M.; Tu, Y.; Euskirchen, G.; Ward, W. W.; Prasher, D. C. Green Fluorescent Protein as a Marker for Gene Expression. *Science* **1994**, *263*, 802−805.

(10) Kanda, T.; Sullivan, K. F.; Wahl, G. M. Histone−GFP Fusion Protein Enables Sensitive Analysis of Chromosome Dynamics in Living Mammalian Cells. *Curr. Biol.* **1998**, *8*, 377−385.

(11) Schneider, N.; Schwartz, J. M.; Köhler, J.; Becker, M.; Schwarz, H.; Gerisch, G. Golvesin-GFP Fusions as Distinct Markers for Golgi and Post-Golgi Vesicles in Dictyostelium Cells. *Biol. Cell* **2000**, *92*, 495−511.

(12) Voliani, V.; Bizzarri, R.; Nifosì, R.; Abbruzzetti, S.; Grandi, E.; Viappiani, C.; Beltram, F. Cis−Trans Photoisomerization of Fluorescent-Protein Chromophores. *J. Phys. Chem. B* **2008**, *112*, 10714−10722.

(13) Abbandonato, G.; Signore, G.; Nifosì, R.; Voliani, V.; Bizzarri, R.; Beltram, F. Cis−Trans Photoisomerization Properties of GFP Chromophore Analogs. *Eur. Biophys. J.* **2011**, *40*, 1205−1214.

(14) Tsien, R. Y. The Green Fluorescent Protein. *Annu. Rev. Biochem.* **1998**, *67*, 509−544.

(15) Marriott, G.; et al. Optical Lock-in Detection Imaging Microscopy for Contrast-Enhanced Imaging in Living Cells. *Proc. Natl. Acad. Sci. U. S. A.* **2008**, *105*, 17789−17794.

(16) Betzig, E.; Patterson, G. H.; Sougrat, R.; Lindwasser, O. W.; Olenych, S.; Bonifacino, J. S.; Davidson, M. W.; Lippincott-Schwartz, J.; Hess, H. F. Imaging Intracellular Fluorescent Proteins at Nanometer Resolution. *Science* **2006**, *313*, 1642−1645.

(17) Zhang, X.; Zhang, M.; Li, D.; He, W.; Peng, J.; Betzig, E.; Xu, P. Highly Photostable, Reversibly Photoswitchable Fluorescent Protein with High Contrast Ratio for Live-Cell Superresolution Microscopy. *Proc. Natl. Acad. Sci. U. S. A.* **2016**, *113*, 10364−10369.

(18) Chen, Y.-C.; Dickson, R. M. Improved Fluorescent Protein Contrast and Discrimination by Optically Controlling Dark State Lifetimes. *J. Phys. Chem. Lett.* **2017**, *8*, 733−736.

(19) Chen, Y.-C.; Sood, C.; Francis, A. C.; Melikyan, G. B.; Dickson, R. M. Facile Autofluorescence Suppression Enabling Tracking of Single Viruses in Live Cells. *J. Biol. Chem.* **2019**, *294*, 19111−19118.

(20) Dean, K. M.; Lubbeck, J. L.; Binder, J. K.; Schwall, L. R.; Jimenez, R.; Palmer, A. E. Analysis of Red-Fluorescent Proteins Provides Insight into Dark-State Conversion and Photodegradation. *Biophys. J.* **2011**, *101*, 961−969.

(21) Hendrix, J.; Flors, C.; Dedecker, P.; Hofkens, J.; Engelborghs, Y. Dark States in Monomeric Red Fluorescent Proteins Studied by Fluorescence Correlation and Single Molecule Spectroscopy. *Biophys. J.* **2008**, *94*, 4103−4113.

(22) Prangsma, J. C.; et al. Quantitative Determination of Dark Chromophore Population Explains the Apparent Low Quantum Yield of Red Fluorescent Proteins. *J. Phys. Chem. B* **2020**, *124*, 1383−1391.

(23) Manna, P.; Hung, S.-T.; Mukherjee, S.; Friis, P.; Simpson, D. M.; Lo, M. N.; Palmer, A. E.; Jimenez, R. Directed Evolution of Excited State Lifetime and Brightness in Fusionred Using a Microfluidic Sorter. *Integrative Biol.* **2018**, *10*, 516−526.

(24) Biteen, J. S.; Thompson, M. A.; Tselentis, N. K.; Bowman, G. R.; Shapiro, L.; Moerner, W. E. Super-Resolution Imaging in Live Caulobacter Crescentus Cells Using Photoswitchable EYFP. *Nat. Methods* **2008**, *5*, 947−949.

(25) Hsiang, J.-C.; Jablonski, A. E.; Dickson, R. M. Optically Modulated Fluorescence Bioimaging: Visualizing Obscured Fluorophores in High Background. *Acc. Chem. Res.* **2014**, *47*, 1545−1554.

(26) Richards, C. I.; Hsiang, J.-C.; Dickson, R. M. Synchronously Amplified Fluorescence Image Recovery (SAFIRe). *J. Phys. Chem. B* **2010**, *114*, 660.

(27) Richards, C. I.; Hsiang, J.-C.; Senapati, D.; Patel, S.; Yu, J.; Vosch, T.; Dickson, R. M. Optically Modulated Fluorophores for Selective Fluorescence Signal Recovery. *J. Am. Chem. Soc.* **2009**, *131*, 4619−4621.

(28) Fan, C.; Hsiang, J. C.; Dickson, R. M. Optical Modulation and Selective Recovery of Cy5 Fluorescence. *ChemPhysChem* **2012**, *13*, 1023−1029.

(29) Demissie, A. A.; Dickson, R. M. Triplet Shelving in Fluorescein and Its Derivatives Provides Delayed, Background-Free Fluorescence Detection. *J. Phys. Chem. A* **2020**, *124*, 1437−1443.

(30) Krause, S.; Carro-Temboury, M. R.; Cerretani, C.; Vosch, T. Probing Heterogeneity of Nir Induced Secondary Fluorescence from DNA-Stabilized Silver Nanoclusters at the Single Molecule Level. *Phys. Chem. Chem. Phys.* **2018**, *20*, 16316−16319.

(31) Jablonski, A. E.; Hsiang, J.-C.; Bagchi, P.; Hull, N.; Richards, C. I.; Fahrni, C. J.; Dickson, R. M. Signal Discrimination between Fluorescent Proteins in Live Cells by Long-Wavelength Optical Modulation. *J. Phys. Chem. Lett.* **2012**, *3*, 3585−3591.

(32) Demissie, A. A.; VanderLaan, D.; Islam, M. S.; Emelianov, S.; Dickson, R. M. Synchronously Amplified Photoacoustic Image Recovery (SAPhIRe). *Photoacoustics* **2020**, *20*, 100198.

(33) Jablonski, A. E.; Vegh, R. B.; Hsiang, J.-C.; Bommarius, B.; Chen, Y.-C.; Solntsev, K. M.; Bommarius, A. S.; Tolbert, L. M.; Dickson, R. M. Optically Modulatable Blue Fluorescent Proteins. *J. Am. Chem. Soc.* **2013**, *135*, 16410−16417.

(34) Chen, Y.-C.; Jablonski, A. E.; Issaeva, I.; Bourassa, D.; Hsiang, J.-C.; Fahrni, C. J.; Dickson, R. M. Optically Modulated Photo-switchable Fluorescent Proteins Yield Improved Biological Imaging Sensitivity. *J. Am. Chem. Soc.* **2015**, *137*, 12764−12767.

(35) You, C.; Zhang, Y.-H. P. Easy Preparation of a Large-Size Random Gene Mutagenesis Library in Escherichia Coli. *Anal. Biochem.* **2012**, *428*, 7−12.

(36) Mamontova, A. V.; Solovyev, I. D.; Savitsky, A. P.; Shakhov, A.; Lukyanov, K. A.; Bogdanov, A. M. Bright GFP with Subnanosecond Fluorescence Lifetime. *Sci. Rep.* **2018**, *8*, 13224−5.

(37) Otwinowski, Z.; Minor, W. Processing of X-Ray Diffraction Data Collected in Oscillation Mode. *Methods Enzymol.* **1997**, *276*, 307−326.

(38) Liebschner, D.; et al. Macromolecular Structure Determination Using X-Rays, Neutrons and Electrons: Recent Developments in Phenix. *Acta Cryst. D, Struct. Biol.* **2019**, *75*, 861−877.

(39) Emsley, P.; Cowtan, K. Coot: Model-Building Tools for Molecular Graphics. *Acta Crystallogr., Sect. D: Biol. Crystallogr.* **2004**, *60*, 2126−2132.

(40) Krissinel, E.; Henrick, K. Secondary-Structure Matching (SSM), a New Tool for Fast Protein Structure Alignment in Three Dimensions. *Acta Crystallogr., Sect. D: Biol. Crystallogr.* **2004**, *60*, 2256−2268.

(41) Schrödinger, L. The Pymol Molecular Graphics System, Version 1.8. 2015.

(42) Agmon, N. Kinetics of Switchable Proton Escape from a Proton-Wire within Green Fluorescence Protein. *J. Phys. Chem. B* **2007**, *111*, 7870−7878.

(43) Phillips, G. N., Jr. Structure and Dynamics of Green Fluorescent Protein. *Curr. Opin. Struct. Biol.* **1997**, *7*, 821−827.

(44) Byrdin, M.; Duan, C.; Bourgeois, D.; Brettel, K. A Long-Lived Triplet State Is the Entrance Gateway to Oxidative Photochemistry in Green Fluorescent Proteins. *J. Am. Chem. Soc.* **2018**, *140*, 2897−2905.

(45) Mohr, M. A.; Kobitski, A. Y.; Sabater, L. R.; Nienhaus, K.; Obara, C. J.; Lippincott-Schwartz, J.; Nienhaus, G. U.; Pantazis, P. Rational Engineering of Photoconvertible Fluorescent Proteins for Dual-Color Fluorescence Nanoscopy Enabled by a Triplet-State Mechanism of Primed Conversion. *Angew. Chem., Int. Ed.* **2017**, *56*, 11628−11633.

(46) Mahoney, D. P.; Demissie, A. A.; Dickson, R. M. Optically Activated Delayed Fluorescence through Control of Cyanine Dye Photophysics. *J. Phys. Chem. A* **2019**, *123*, 3599−3606.

(47) Fleischer, B. C.; Petty, J. T.; Hsiang, J.-C.; Dickson, R. M. Optically Activated Delayed Fluorescence. *J. Phys. Chem. Lett.* **2017**, *8*, 3536−3543.

(48) De Zitter, E.; Hugelier, S.; Duwé, S.; Vandenberg, W.; Tebo, A. G.; Van Meervelt, L.; Dedecker, P. Structure-Function Dataset Reveals Environment Effects within a Fluorescent Protein Model System. *Angew. Chem., Int. Ed.* **2021**, *60*, 10073−10081.

(49) Rekas, A.; Alattia, J.-R.; Nagai, T.; Miyawaki, A.; Ikura, M. Crystal Structure of Venus, a Yellow Fluorescent Protein with Improved Maturation and Reduced Environmental Sensitivity. *J. Biol. Chem.* **2002**, *277*, 50573−50578.

(50) Andresen, M.; et al. Structure and Mechanism of the Reversible Photoswitch of a Fluorescent Protein. *Proc. Natl. Acad. Sci. U. S. A.* **2005**, *102*, 13070−13074.